Neural field theory of evoked response potentials in a spherical brain geometry

K. N. Mukta,* Xiao Gao, and P. A. Robinson
School of Physics, University of Sydney, New South Wales 2006, Australia
and Center for Integrative Brain Function, University of Sydney, New South Wales 2006, Australia

(Received 3 December 2018; published 12 June 2019)

Evoked response potentials (ERPs) are calculated in spherical and planar geometries using neural field theory of the corticothalamic system. The ERP is modeled as an impulse response and the resulting modal effects of spherical corticothalamic dynamics are explored, showing that results for spherical and planar geometries converge in the limit of large brain size. Cortical modal effects can lead to a double-peak structure in the ERP time series. It is found that the main difference between infinite planar geometry and spherical geometry is that the ERP peak is sharper and stronger in the spherical geometry. It is also found that the magnitude of the response decreases with increasing spatial width of the stimulus at the cortex. The peak is slightly delayed at large angles from the stimulus point, corresponding to group velocities of 6–10 m s^{-1}. Strong modal effects are found in the spherical geometry, with the lowest few modes sufficing to describe the main features of ERPs, except very near to spatially narrow stimuli.

DOI: 10.1103/PhysRevE.99.062304

I. INTRODUCTION

Transient electrical responses to brief sensory stimuli are called evoked response potentials (ERPs). These responses are recorded from the scalp or within the brain and are superimposed on ongoing brain activity [1,2]. Evoked potentials consist of "early" components (20–60 ms after the stimulus) that are often ascribed to initial processing of the stimulus, but their most prominent components are the so called late evoked response potentials (ERPs) [3–5], which begin about 100 ms after the onset of the stimulus, have the appearance of a damped oscillatory waveform lasting ≈200 ms, and resemble EEGs in amplitude (≈10 μV) and frequency content (≈1–20 Hz) [1].

Physiology-based neural field theory (NFT) has been successfully used to analyze brain activity [6–26] accounting for a wide range of quantitative experimental observations of various signals that are ultimately generated by neural activity [2,7,27–30], including spontaneous EEG, steady-state evoked potentials, seizures, brain network structure, and dynamics [31–34], and a range of arousal-state phenomena [28,35–37]. NFT modeling of ERPs [38,39] has enabled the underlying physiological parameters that correspond to various states to be deduced, and the parameters underlying ERPs to inferred [2,27,34,40–44]. Previous work [1,2,45] studied ERPs in a planar geometry using a well-established neural field corticothalamic model [10], show that all ERP components can be accounted for as the result of a single impulse occurring in a system whose spontaneous EEG characteristics can also be reproduced by the same model. Our prior work [2] developed a physiology-based method to analyze ERPs and their dependence on corticothalamic system. Using a planar model yielded excellent fits to experimental auditory evoked potential (AEP) data for around 1500 subjects, and the parameters of the fits were used to constrain the physiological basis of AEP generation [3,4]; notably, the inferred parameters fell within physiologically realistic ranges without additional constraints [2].

The real brain is not planar; rather, each hemisphere has a spherical topology and is convoluted. Some work has analyzed the EEG signals produced by brain activity using a spherical model of the skull and other tissues, including volume conduction [46–48], but did not consider individual brain hemispheres or the thalamus, as needed for more general brain-activity models [49,50]. Hence, here we use a spherical geometry to model ERPs on one brain hemisphere, using spherical harmonic analysis. Spherical harmonics are well understood and have been applied to the approximation of brain surfaces [51] and many other applications such as spatial filtering, calculation of EEG coherence on the scalp [52], and brain imaging [53–59]. This extends our previous work, which showed that eigenmodes of a single brain hemisphere are close analogs of spherical harmonics [50], and examined the effects of spherical geometry on activity measures such as spectra, coherence, and correlations [10,49,60]. The close parallels between modes in the spherical and convoluted cases [50,61] make the present analysis a useful bridge between analytically tractable cases and the fully general case, which must be treated numerically. In particular, it provides a reference point to assist in understanding the properties of the more complicated modes on a fully convoluted cortex.

The structure of this paper is as follows. After briefly reviewing the neural field model of the corticothalamic system in Sec. II, we derive ERPs in planar geometry. In Sec. III we derive ERPs in spherical geometry. In Sec. IV we discuss the ERPs, modal effects, and numerical analysis. Finally, Sec. V presents the conclusions.

*Corresponding author: muktaphy@gmail.com

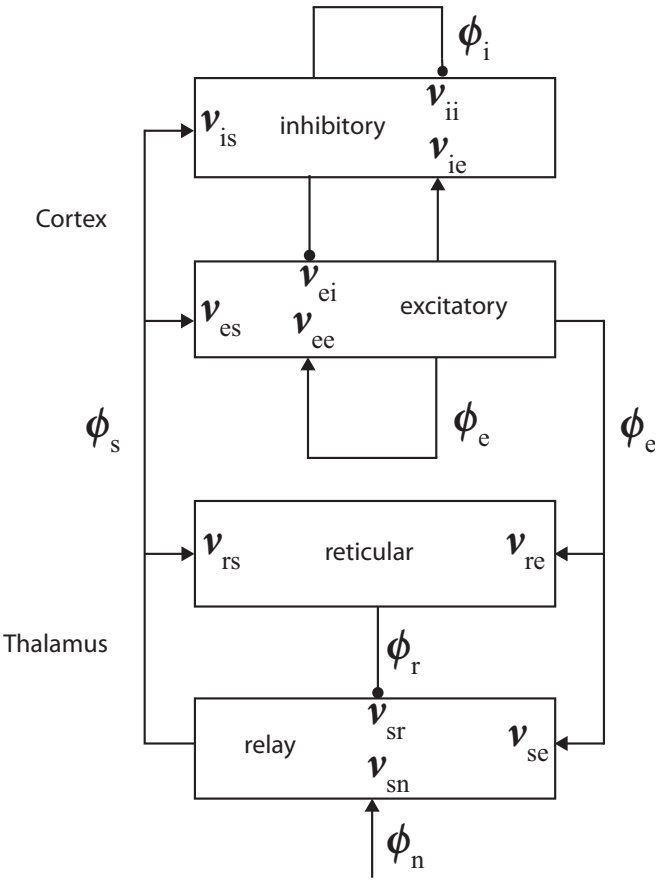

FIG. 1. Schematic diagram of corticothalamic neural field model of the system. The neural populations shown are cortical excitatory e, cortical inhibitory i, thalamic reticular r, and thalamic relay s. Each parameter ν_{ab} from Eq. (2) quantifies the connection to population a from population b. Excitatory connections are shown with pointed arrowheads and inhibitory connections are shown with round arrowheads.

II. NEURAL FIELD THEORY OF THE CORTICOTHALAMIC SYSTEM

In this section we start with a brief review of the neural field corticothalamic model that we employ, and the transfer function for neural activity, in general, and in infinite and finite planar geometries [10,11,35].

A. Corticothalamic model

It is well-known the corticothalamic system is principally responsible for generation of observed ERP signals [1,2,62], although its activity is influenced by other brain structures. Therefore, we use a physiology-based neural field model of the brain's electrical activity to predict and analyze ERPs. Such models of the brain have been developed and used over several decades [7,9,11,19,46,63–69]. The model used here has been widely employed in previous work [10,11], and incorporates the populations and connections shown in Fig. 1: excitatory (e) and inhibitory (i) cortical neurons, thalamic relay neurons (s), thalamic reticular neurons (r), and sensory inputs (n) [10,12]. As noted in Sec. I, the predictions of this model have been verified against many types of EEG phenomena as well as independent physiological measurements [10,35,36,60,70–73].

The state of given population of neurons is determine by the activity of all populations that synapse onto that population, including activity from self-connections. Hence, the net effect P_a on the activity of neurons of population a by all populations of neurons b is given by

$$P_a(\mathbf{r},t) = \sum_b \nu_{ab}\phi_b(\mathbf{r}, t-\tau_{ab}), \tag{1}$$

with [10,11] $\nu_{ab} = s_{ab}N_{ab}$, where N_{ab} is the mean number of synapses to neurons of type a from type b, s_{ab} is the mean time-integrated strength of soma response per incoming spike, ϕ_b is the activity (expressed as the mean rate of action potentials) arising from neurons of type b, τ_{ab} is the discrete delay for signals to propagate to population a from b when they are in different structures (this is zero for all connections except $\tau_{es} = \tau_{se} = \tau_{re} = t_0/2$), and the sum is over all populations of neurons that have connections to neurons of population a [12,28,35].

The effect of synaptic activity on the mean postsynaptic populations membrane potential involves the kinetics of the neurotransmitter and the electrical properties of dendrites, its receptor, and soma capacitance, all of whose dynamics attenuate high-frequency components of the signal. This dynamics can be approximated by convolution kernel

$$L(t) = \frac{\alpha\beta}{\beta-\alpha}(e^{-\alpha t} - e^{-\beta t}), \tag{2}$$

for $t \geqslant 0$, with $L = 0$ for $t < 0$, where $1/\beta$ and $1/\alpha$ are the rise time and decay time constants, respectively [2,11]. The membrane potential V_a (relative to resting) for a population of neurons is then approximated by a convolution of net activity P_a and the kernel $L(t)$, with

$$V_a(\mathbf{r},t) = \int_{-\infty}^{t} L(t-t')P_a(\mathbf{r},t')dt'. \tag{3}$$

The activity of a population of neurons exhibits a sigmoid response to increasing mean membrane depolarization, because its cells have distribution of the different between individual soma voltage and threshold potential due to variations in environment and membrane properties. This response is approximated by [2,9,11]

$$Q_a(\mathbf{r},t) = \frac{Q_{\max}}{1+\exp\{-C(V_a-\theta_a)/\sigma_a\}}, \tag{4}$$

where Q_a is the mean firing rates, $Q_{\max}$ is the maximum firing rate, θ_a is the mean neural firing threshold, σ_a is the standard deviation (SD) of the derivative, and $C = \pi/\sqrt{3}$.

Treating the EEG signal as being the result of small perturbations about a steady state, the response function becomes [2,45]

$$Q_a(\mathbf{r},t) \approx Q_a^{(0)} + \rho_a\left[V_a(\mathbf{r},t) - V_a^{(0)}\right], \tag{5}$$

where

$$\rho_a \equiv \frac{dQ_a}{dV_a} = \frac{CQ_a}{\sigma_a}\left(1 - \frac{Q_a}{Q_a^{\max}}\right), \tag{6}$$

and is evaluated at steady state. It is not necessary to determine the steady state firing rate $Q_a^{(0)}$, because only perturbations to

this value are used in the model. Henceforth, the quantities Q_a, ϕ_a, and V_a denote perturbations from their fixed points.

To relate the neuronal activity ϕ_a to the average membrane potential Q_a, we use a damped wave equation to approximate the propagation of neuronal activity in the cortex [10,11,72]. Hence,

$$D_\alpha \phi_a(\mathbf{r}, t) = Q_a(\mathbf{r}, t), \tag{7}$$

$$D_\alpha = \frac{1}{\gamma_a^2}\left[\frac{\partial^2}{\partial t^2} + 2\gamma_a^2\frac{\partial}{\partial t} + \gamma_a^2 - v_a^2\nabla^2\right], \tag{8}$$

where $\gamma_a = v_a/r_a$ is the temporal damping rate, v_a is the axonal propagation velocity, and r_a is the characteristic range of axons for neurons of population a [11]. Since cortical inhibitory neurons have short ($\sim 10^{-4}$ m) axons, we assume $r_i \approx 0$, and hence $D_i \approx 1$ [11]; the same approximation can be made for intrathalamic connections, so $D_s \approx D_r \approx 1$ [2]. Equation (8) with $a = e$ embodies corticocortical via the long-range white matter connections of cortical pyramidal cells.

To obtain the transfer function, we first Fourier transform Eqs. (2)–(6). We define the Fourier transform of a function $g(t)$ as

$$g(\omega) = \int_{-\infty}^{\infty} g(t)e^{i\omega t}dt. \tag{9}$$

Assuming that a signal traveling from the thalamus to cortex, or vice versa, takes a time $t_0/2$, we find that Eq. (2) becomes

$$P_e(\mathbf{k}, \omega) = \nu_{ee}\phi_e + \nu_{ei}\phi_i + \nu_{es}e^{i\omega t_0/2}\phi_s, \tag{10}$$

$$P_i(\mathbf{k}, \omega) = \nu_{ii}\phi_i + \nu_{ie}\phi_e + \nu_{is}e^{i\omega t_0/2}\phi_s, \tag{11}$$

$$P_s(\mathbf{k}, \omega) = \nu_{se}\phi_e e^{i\omega t_0/2} + \nu_{sr}\phi_r + \nu_{sn}\phi_n, \tag{12}$$

$$P_r(\mathbf{k}, \omega) = \nu_{re}\phi_e e^{i\omega t_0/2} + \nu_{rs}\phi_s, \tag{13}$$

where $\mathbf{k}$ is the wave number and ω is the frequency. Equations (3)–(5) and (7) become

$$L(\omega) = \left(1 - \frac{i\omega}{\beta}\right)^{-1}\left(1 - \frac{i\omega}{\alpha}\right)^{-1}, \tag{14}$$

$$V_a(\mathbf{k}, \omega) = L(\omega)P_a(\mathbf{k}, \omega), \tag{15}$$

$$Q_a(\mathbf{k}, \omega) = \rho_a V_a(\mathbf{k}, \omega), \tag{16}$$

$$D_a(\mathbf{k}, \omega)\phi_a(\mathbf{k}, \omega) = Q_a(\mathbf{k}, \omega), \tag{17}$$

$$D_e(\mathbf{k}, \omega) = k^2 r_e^2 + (1 - i\omega/\gamma_e)^2, \tag{18}$$

$$D_i = D_s = D_r = 1. \tag{19}$$

B. ERP in planar geometry

In this section we briefly derive the form of the ERPs for infinite planar geometry, following Ref. [2]. First, we derive the form of the transfer function, then we approximate the incoming stimulus, and finally we derive the form of the ERPs.

1. Transfer function

The scalp potential measured using EEG techniques is directly related to ϕ_e [2,46,74] and stimulus is defined as ϕ_n. To determine the evoked activity from a stimulus ϕ_n requires the transfer function ϕ_e/ϕ_n. The transfer function ϕ_e/ϕ_n, which is the cortical excitatory response per unit external stimulus, including the relative phase via its complex value [10], and is found by eliminating P, V, and Q from Eqs. (10) to (19). Assuming random cortical connectivity (i.e., $G_{ab} = G_{cb}$ for all combinations where a, b, c are either e or i [2]), the transfer function for an impulse traveling directly from the thalamus to the cortex is given by [2,45]

$$T_{en}(\mathbf{k}, \omega) = \frac{\phi_e(\mathbf{k}, \omega)}{\phi_n(\mathbf{k}, \omega)}, \tag{20}$$

$$= \frac{\mathcal{I}}{\mathcal{M}_c - \mathcal{M}_t}, \tag{21}$$

with

$$\mathcal{I} = \frac{e^{i\omega t_0/2}L^2 G_{esn}}{1 - L^2 G_{srs}}, \tag{22}$$

the modulation of this signal by cortical feedback is

$$\mathcal{M}_c = D_e(1 - LG_{ei}) - LG_{ee}, \tag{23}$$

and the modulation by corticothalamic loops is

$$\mathcal{M}_t = \frac{e^{i\omega t_0}(L^2 G_{ese} + L^3 G_{esre})}{1 - L^2 G_{srs}}, \tag{24}$$

where G_{ab} is the gain

$$G_{ab} = \frac{\partial Q_a}{\partial Q_b} = \rho_a N_{ab} s_b = \rho_a \nu_{ab}, \tag{25}$$

where the derivative is evaluated at the fixed point. The net gain of more than two populations of neurons connected serially is simply the product of the separate gains, and we write such compound gains as $G_{ab}G_{bc} = G_{abc}$, for example. In the reduced model, the five relevant linear gains that result are G_{ee}, G_{ii}, G_{ese}, G_{esre}, and G_{srs}. Each of which is the ratio of the change in the activity of neurons of population a in response to a unit change in the incoming activity from neurons of population b.

A stimulus $\phi_n(\mathbf{k}, \omega)$ of angular frequency $\omega = 2\pi f$ (where f is the usual frequency in Hz) and wave vector $\mathbf{k} = 2\pi/\lambda$ (where λ is the wavelength) has the transfer function to $\phi_e(\mathbf{k}, \omega)$,

$$T_{en}(\mathbf{k}, \omega) = \frac{A(\omega)}{k^2 r_e^2 + q^2 r_e^2}, \tag{26}$$

where

$$A(\omega) = \frac{e^{i\omega t_0/2}L^2 G_{esn}}{(1 - L^2 G_{srs})(1 - G_{ei}L)}, \tag{27}$$

with

$$q^2 r_e^2 = \left(1 - \frac{i\omega}{\gamma_e}\right)^2 - \frac{1}{1 - G_{ei}L} \times \left\{LG_{ee} + \frac{[L^2 G_{ie} + L^3 G_{erse}]e^{i\omega t_0}}{1 - L^2 G_{srs}}\right\}. \tag{28}$$

According to our prior work [49], for an infinite planar brain geometry, the spatial eigenmodes labeled $\mathbf{k}$ are Fourier

modes; i.e.,

$$y_\eta(\mathbf{r}) = \exp(i\mathbf{k}\cdot\mathbf{r}), \tag{29}$$

$$k_\eta^2 r_e^2 = k^2 r_e^2, \tag{30}$$

where $\mathbf{k}$ is the wave vector. In a finite planar geometry, we approximate the cortex as a rectangular sheet of size $L_x \times L_y$ and the modes have the form of the first of Eq. (29) but with $\mathbf{k} = \mathbf{k}_{mn} = (k_x, k_y)$ satisfying

$$k_x = \frac{2\pi m}{L_x}, \tag{31}$$

$$k_y = \frac{2\pi n}{L_y}, \tag{32}$$

where m and n are arbitrary integers.

2. Stimulus

We now calculate the response in ϕ_e to a change in the input stimulus ϕ_n. We first linearize the response relative to an assumed steady state. After that we Fourier transform the linearized equations and calculate the transfer function. We approximate the incoming stimulus from the sensory neurons as a Gaussian in both space and time. Such a stimulus has the normalized form [2]

$$\phi_n(\mathbf{r}, t) = \frac{1}{t_s\sqrt{2\pi}}\frac{1}{\pi r_s^2}\exp\left[-\frac{1}{2}\left(\frac{t - t_{os}}{t_s}\right)^2\right] \times \exp\left[-\left(\frac{|\mathbf{r} - \mathbf{r}_{os}|}{r_s}\right)^2\right], \tag{33}$$

where t_s is the characteristics duration of the stimulus, t_{os} is the stimulus onset time, r_s is the spatial width of the stimulus at cortex, and $\mathbf{r}_{os}$ is the offset of the center of the stimulus from the point of measurement. The Fourier transform of this function is

$$\phi_n(\mathbf{k}, \omega) = \exp\left(-\omega^2 t_s^2/2\right)\exp(i\omega t_{os}) \times \exp\left(-k^2 r_s^2/4\right)\exp(-i\mathbf{k}\cdot\mathbf{r}_{os}). \tag{34}$$

3. Evoked potential

To calculate the response of the cortical neurons ϕ_e to the input stimulus ϕ_n, we must inverse Fourier transform the product of Eqs. (20) and (34):

$$R(\mathbf{r}, t) = \frac{1}{(2\pi)^3}\iint e^{-i\omega t}T_{en}(\mathbf{k}, \omega) \times \phi_n(\mathbf{k}, \omega)e^{i\mathbf{k}\cdot\mathbf{r}}\, d\omega\, d^2\mathbf{k}. \tag{35}$$

Considering first the spatial inverse Fourier transform, we find

$$R(\mathbf{r}, \omega) = \frac{1}{(2\pi)^2}\int T_{en}(\mathbf{k}, \omega)\phi_n(\mathbf{k}, \omega)e^{i\mathbf{k}\cdot\mathbf{r}}d^2\mathbf{k}, \tag{36}$$

$$= \frac{1}{(2\pi)^2}\int T_{en}(\mathbf{k}, \omega)\mathrm{e}^{-k^2 r_s^2/4} \times e^{-i\mathbf{k}\cdot\mathbf{r}_{os}}e^{i\mathbf{k}\cdot\mathbf{r}}d^2\mathbf{k}, \tag{37}$$

$$= \frac{1}{(2\pi)^2}\int_0^\infty T_{en}(\mathbf{k}, \omega)e^{-k^2 r_s^2/4} \times \int_0^{2\pi} e^{ik|\mathbf{r}-\mathbf{r}_{os}|\cos\theta}d\theta k dk, \tag{38}$$

$$= \frac{1}{2\pi}\int_0^\infty T_{en}(\mathbf{k}, \omega)e^{-k^2 r_s^2/4} \times J_0(k|\mathbf{r} - \mathbf{r}_{os}|)k dk, \tag{39}$$

where J_0 is a Bessel function of the first kind [75].

The Fourier transform on a 2D finite plane is the same as the infinite 2D plane, except that the integrals over $\mathbf{k}$ are replaced by sums over the allowed values, with

$$\int \frac{d^2\mathbf{k}}{(2\pi)^2} \to \frac{1}{L_x L_y}\sum_{m=-\infty}^{\infty}\sum_{n=-\infty}^{\infty}. \tag{40}$$

So, we can write

$$f(\mathbf{r}, \omega) = \frac{1}{L_x L_y}\sum_{m=-\infty}^{\infty}\sum_{n=-\infty}^{\infty} f(\mathbf{k}_{mn}, \omega)\exp(i\mathbf{k}_{mn}\cdot\mathbf{r}), \tag{41}$$

$$f(\mathbf{k}_{mn}, \omega) = \int f(\mathbf{r}, \omega)\exp(-i\mathbf{k}_{mn}\cdot\mathbf{r})d^2\mathbf{r}. \tag{42}$$

To using infinite boundary conditions, one can also define a 2D rectangular cortex of dimensions $L_x \times L_y$ and sum over discrete wave numbers corresponding to the modes of the system. In this case, $R(\mathbf{r}, \omega)$ can be evaluated using [2]

$$R(\mathbf{r}, \omega) = \frac{1}{L_x L_y}\sum_{m,n=-\infty}^{\infty}\frac{\phi_e(\mathbf{k}_{mn}, \omega)}{\phi_n(\mathbf{k}_{mn}, \omega)} \times e^{-k^2 r_s^2/4}e^{i\mathbf{k}_{mn}\cdot(\mathbf{r}-\mathbf{r}_{os})}, \tag{43}$$

where

$$\mathbf{k}_{mn} = \left(\frac{2\pi m}{L_x}, \frac{2\pi n}{L_y}\right), \tag{44}$$

and $k_{mn} = |\mathbf{k}_{mn}|$.

Finally, an inverse temporal Fourier transform is performed to obtain

$$R(\mathbf{r}, t) = \frac{1}{2\pi}\int R(\mathbf{r}, \omega)\exp\left(-\omega^2 t_s^2/2\right) \times \exp[-i\omega(t - t_{os})]d\omega. \tag{45}$$

III. ERP IN SPHERICAL GEOMETRY

In this section we derive the form of the ERP in a spherical geometry ERP's one brain hemisphere. We begin with the form of the transfer function, then approximate the stimulus, and finally calculate the form of the ERP. We then discuss the predictions of the model and numerically investigate the results, comparing them with planar geometry in the relevant limit.

A. Transfer function

As in our prior work [49] once we have eigenvalue k_η^2 we can write the general transfer function as

$$T\left(k_\eta^2,\omega\right)=\frac{A(\omega)}{k_\eta^2 r_e^2+q^2 r_e^2}, \tag{46}$$

where $A(\omega)$ is defined in Eq. (27).

This is an approximation that has been extensively used to represent EEG activity on the scalp [46,50], albeit most often treating the whole brain, skull, and scalp as nested spheres; an exception was Ref. [50], which analyzed the activity eigenmodes of a single hemisphere of the brain.

In the case of a sphere of radius R_s, the eigenmodes are

$$y_{\ell m}(\vartheta,\varphi)=Y_{\ell m}(\vartheta,\varphi), \tag{47}$$

where η has been replaced by ℓ and m, and the $Y_{\ell m}$ are the real spherical harmonics, the position is parametrized by spherical coordinates ϑ and φ, with

$$Y_{\ell m}(\vartheta,\varphi)=\begin{cases} c_{\ell m}P_\ell^{|m|}(\cos\vartheta)\sin(|m|\varphi), & -\ell\leqslant m\leqslant -1,\\ 2^{-1/2}c_{\ell m}P_\ell^0(\cos\vartheta), & m=0,\\ c_{\ell m}P_\ell^{|m|}(\cos\vartheta)\cos(|m|\varphi), & 1\leqslant m\leqslant \ell,\end{cases} \tag{48}$$

where

$$c_{\ell m}=\left[\frac{2\ell+1}{2\pi}\frac{(\ell-|m|)!}{(\ell+|m|)!}\right]^{1/2}.$$

For a sphere,

$$k_{\ell m}^2 r_e^2=\frac{r_e^2}{R_s^2}\ell(\ell+1). \tag{49}$$

Equation (49) shows that the eigenvalues depend only on the angular momentum mode number $\ell=0,1,...$ and are independent of the azimuthal mode number $m=-\ell,...,\ell$.

The spectral decomposition of the activity is then

$$\phi_e(\vartheta,\varphi,\omega)=\sum_{\ell=0}^{\infty}\sum_{m=-\ell}^{\ell}T(\ell,m,\omega)\times\phi_n(\ell,m,\omega)Y_{\ell m}(\vartheta,\phi), \tag{50}$$

with [49]

$$T(\ell,m,\omega)=\frac{\phi_e(\ell,m,\omega)}{\phi_n(\ell,m,\omega)}=\frac{A(\omega)}{\ell(\ell+1)r_e^2/R_s^2+q^2r_e^2}. \tag{51}$$

B. Stimulus

To calculate $\phi_e(\vartheta,\varphi,t)$ from Eq. (51) we need to specify a stimulus, as we did in planar geometry in Sec. II B. We approximate the incoming stimulus arising from sensory neurons as being approximately Gaussian in both space and time and choose the analytically tractable form

$$\phi_n(\vartheta,\varphi,t)=\frac{\mathcal{D}}{t_s\sqrt{2\pi}}\exp\left\{-\frac{1}{2}\left(\frac{t-t_{os}}{t_s}\right)^2\right\}\exp\left(\frac{\cos\vartheta}{\theta_s^2}\right), \tag{52}$$

with $\mathcal{D}=[4\pi\theta_s^2\sinh(\theta_s^{-2})]^{-1}$; again, this form is normalized to have unit integral. This angular form can be approximated at small ϑ as

$$\exp\left(\theta_s^{-2}\cos\vartheta\right)\approx\exp\left(\theta_s^{-2}\right)\exp\left(-\frac{\vartheta^2}{2\theta_s^2}\right), \tag{53}$$

which is thus verified to be approximately Gaussian.

Any continuous bounded function on a sphere can be expanded in terms of real-valued spherical harmonics. So a spherical harmonic transformation and a Fourier transform t of Eq. (52) yield

$$\phi_n(\ell,m,\omega)=\iiint\phi_n(\vartheta,\varphi,t)e^{i\omega t}dt\times Y_{\ell m}(\vartheta,\varphi)\sin\vartheta\,d\vartheta\,d\varphi, \tag{54}$$

with ℓ being a nonnegative integer and $-\ell\leqslant m\leqslant\ell$. The integral in Eq. (54) extends over the whole sphere, giving

$$\phi_n(\ell,0,\omega)=\frac{\mathcal{D}}{t_s\sqrt{2\pi}}\iiint\exp\left\{-\frac{1}{2}\left(\frac{t-t_{os}}{t_s}\right)^2\right\}e^{i\omega t}dt\times\exp\left(\frac{\cos\vartheta}{\theta_s^2}\right)Y_{\ell0}(\vartheta,\varphi)\sin\vartheta\,d\vartheta\,d\varphi. \tag{55}$$

Because ϕ_n^2 does not depend on φ, only the $Y_{\ell0}$ are relevant and these only depend on ϑ.

Equation (55) can then be written as a product of two factors, P_1' and P_2', with

$$P_1'=\frac{1}{t_s\sqrt{(2\pi)}}\int\exp\left\{-\frac{1}{2}\left(\frac{t-t_{os}}{t_s}\right)^2\right\}e^{i\omega t}dt, \tag{56}$$

$$=\exp\left(-\omega^2t_s^2/2\right)\exp(i\omega t_{os}), \tag{57}$$

$$P_2'=\int\exp\left(\frac{\cos\vartheta}{\theta_s^2}\right)Y_{\ell0}(\vartheta,\varphi)\sin\vartheta\,d\vartheta\,d\varphi, \tag{58}$$

$$=\int_{-1}^{1}2\pi\exp\left(\frac{x}{\theta_s^2}\right)P_\ell(x)\sqrt{\frac{2\ell+1}{4\pi}}dx, \tag{59}$$

where $x=\cos\vartheta$. Using

$$\int_{-a}^{a}\exp(-\rho x)P_n\left(\frac{x}{a}\right)dx=(-1)^n\sqrt{\frac{2\pi a}{\rho}}I_{n+1/2}(a\rho), \tag{60}$$

$$\int_{-a}^{a}\exp(\rho x)P_n\left(\frac{x}{a}\right)dx=\sqrt{\frac{2\pi a}{\rho}}I_{n+1/2}(a\rho), \tag{61}$$

([76] Sec. 2.17.5, p. 428), where $I_{n+1/2}$ is modified Bessel function [75], we obtain

$$P_2'=\pi\sqrt{2}\theta_s\sqrt{2\ell+1}\,I_{\ell+1/2}\left(\frac{1}{\theta_s^2}\right). \tag{62}$$

Substituting Eqs. (57) and (62) into Eq. (55) we find

$$\phi_n(\ell,m,\omega)=\frac{1}{2\sqrt{2}\theta_s\sinh(\theta_s^{-2})}\exp\left(-\frac{1}{2}\omega^2t_s^2\right)\times\exp(i\omega t_{os})\sqrt{2\ell+1}I_{\ell+1/2}\left(\frac{1}{\theta_s^2}\right). \tag{63}$$

C. Evoked response potential

To calculate the response ϕ_e evoked by a change in the input stimulus ϕ_n, we inverse Fourier transform to the time domain; Eqs. (63) and (51) yield

$$R(\vartheta,\varphi,t)=\frac{1}{2\pi R_s^2}\sum_{\ell=0}^{\infty}\sum_{m=-\ell}^{\ell}\int T(\ell,m,\omega)\phi_n(\ell,m,\omega)\times Y_{\ell m}(\vartheta,\varphi)\mathrm{e}^{-i\omega t}d\omega. \quad (64)$$

Considering a sphere of radius R_s, $R(\vartheta,\phi,\omega)$ can be evaluated using

$$R(\vartheta,\varphi,\omega)=\frac{1}{R_s^2}\sum_{\ell=0}^{\infty}\sum_{m=-\ell}^{\ell}T(\ell,m,\omega)\times\phi_n(\ell,m,\omega)Y_{\ell m}(\vartheta,\varphi), \quad (65)$$

$$=\frac{A(\omega)}{4\sqrt{2\pi}R_s^2}\frac{1}{\theta_s\sinh(\theta_s^{-2})}\sum_{\ell=0}^{\infty}\frac{2\ell+1}{\ell(\ell+1)r_e^2/R_s^2+q^2r_e^2}\times I_{\ell+1/2}\left(\frac{1}{\theta_s^2}\right)P_\ell(\cos\vartheta). \quad (66)$$

Finally, to obtain the ERP waveform $R(\vartheta,\varphi,t)$ we perform an inverse Fourier transform to the time domain [2]

$$R(\vartheta,\varphi,t)=\frac{1}{2\pi}\int R(\vartheta,\varphi,\omega)\mathrm{e}^{-\omega^2t_s^2/2}\times\exp[-i\omega(t-t_{os})]d\omega. \quad (67)$$

IV. RESULTS

Our prior work [2] analyzed and discussed ERPs in planar geometry using NFT. In this section we explore and analyze the modal form of ERP in a spherical geometry. We plotted an example of a ERP time series for planar geometry and compare with the ERP time series for spherical geometry. We also explore and analyze the modal decomposition of the ERP in a spherical geometry.

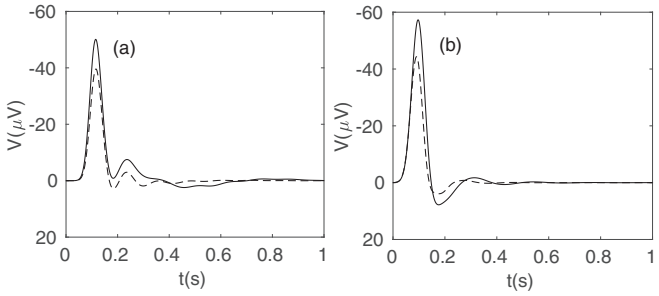

FIG. 2. Theoretical ERP time series for the parameters in Table I from Eqs (45) and (67) for infinite planar (dashed line) and spherical geometries (solid line). (a) Sleep state. (b) Wake state.

In the examples below we normalize all our results by multiplying $R(\vartheta,\varphi,t)$ by a constant factor such that outcomes match typical experimental values in μV [2].

A. ERPs in planar and spherical geometries

In this subsection we compare ERPs numerically in infinite planar geometry and spherical geometry to show how ERPs depend on the geometry, particularly via the discreteness of modes in the finite case. Figure 2 shows examples of ERP time series for infinite planar and spherical geometries, obtained from Eqs. (45) and (67) for the parameters listed in the Table I. In Fig. 2(a), the dashed line for the infinite planar geometry shows a sharp negative peak which decays rapidly due to rapid damping. The response onset is delayed with respect to the stimulus because of the time taken to travel from thalamus to cortex. The ERP time series decays from an initial amplitude of around $-38\,\mu$V and the initial decay time is 0.07 s.

In Fig. 2(a), the ERP time series in a spherical geometry is shown by the solid line for $\vartheta=0^\circ$, $\theta_s=3^\circ$, and $R_s=0.1$ m, these parameters are chosen to keep consistency with width r_s of the planar geometry where $r_s=\theta_sR_s$. From the figure we again see sharp negative peak but stronger than infinite planar geometry after a $\sim$0.04 s delay, because only a modest

TABLE I. Nominal corticothalamic model parameter values from previous work [2,45] where first column shows the symbol for the quantity in the second column. The third, fourth, and fifth columns show the values of the quantity in sleep and wake, and its units, respectively.

Symbol	Quantity	Value (Sleep)	Value (Wake)	Unit
α	Synaptodendritic decay rate	45	83	s^{-1}
β	Synaptodendritic rise rate	185	769	s^{-1}
t_0	Corticothalamic loop delay	0.085	0.064	s
γ_e	Cortical damping rate	116	200	s^{-1}
r_e	Excitatory axon range	0.086	0.086	m
G_{ee}	Excitatory cortical gain	15	3.1	—
G_{ii}	Inhibitory cortical gain	−17.5	−10.8	—
G_{ese}	Excitatory cortical gain	12.3	0.8	—
G_{esre}	Excitatory inhibitory gain	−13.0	−7.88	—
G_{srs}	Intrathalamic gain	−0.7	−0.8	—
R_s	Radius of sphere	0.1	0.1	m
t_{os}	Stimulus onset	0.05	0.05	s
t_s	Stimulus duration	0.019	0.023	s
r_{os}	Stimulus point	0.14	0.14	m
r_s	Stimulus width	0.005	0.005	m

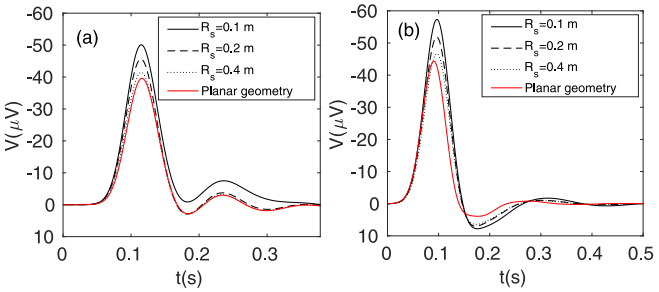

FIG. 3. Theoretical ERP time series for various R_s in spherical geometry from Eq. (67) for increasing R_s at $\vartheta = 0^\circ$ for the parameters in Table I, as indicated in the legend. (a) Sleep state. (b) Wake state.

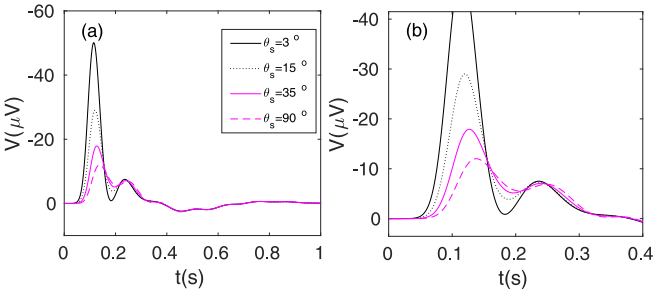

FIG. 4. Model ERP time series at $\vartheta = 0^\circ$ in spherical geometry for various θ_s for the parameters in Table I. (a) ERP time series. (b) Expanded view of (a) showing early times.

number of modes contribute strongly, as in the planar case [49]. The initial negative amplitude $-48\,\mu V$ which rapidly decays with initial decay time $\sim$0.07 s. After time 0.23 s we see that amplitude decays rapidly due to the rapid damping of the slow wave part of the response and after 1 s the amplitude is negligible.

Figure 2(b) shows an ERP time series for a wake state in spherical and infinite planar geometries [2] shown by solid and dashed lines, respectively. In this case we also get a sharp negative peak in the ERP time series for the infinite planar case. For infinite planar geometry the initial negative amplitude of ERP time series decays from $-47\,\mu$V with initial decay time $\sim$0.06 s. Figure 2(b) shows ERP time series for wake state in the spherical geometry and the initial amplitude of ERP time series decays from $-61\,\mu$V with an initial decay time of $\sim$0.08 s.

The main difference between the infinite planar geometry and spherical geometry in Fig. 2 is that the negative peak at $t \approx 0.07$ s is sharper and stronger in the spherical geometry, due to the strong role of the uniform mode ($\ell = 0$) when energy is partitioned into discrete modes, the lowest of which concentrate a significant fraction of the energy in phase. We find that for small R_s in the spherical geometry, the ERP amplitude is high but decreases with R_s since there is a decrease of fractional energy in the $\ell = 0$ mode, because of the term in the denominator $\ell(\ell+1)r_e^2/R_s^2$.

In Fig. 3 we explore how the spherical ERP converges to the planar limit with increasing R_s and $r_s = \theta_s R_s$ to keep the physical widths equal in this limit for different θ_s. Considering both spherical and planar cases, we must relate r and ϑ via $r = R_s\vartheta$. To examine convergence between spherical and planar geometries we then increase R_s, and decrease θ_s accordingly, with $r_s = R_s\theta_s$, so the physical width in planar geometry equals that in the spherical geometry. In Fig. 3(a) we observe that as $R_s \to \infty$, the spherical and infinite planar responses rapidly approach one another as the sum in Eq. (67) better approximates the integral in Eq. (45) for the ERP in an infinite planar geometry. Figure 3(b) shows that spherical and infinite planar cases also converge as $R_s \to \infty$ in the wake state.

B. Dependence on θ_s

This subsection examines how the ERP time series depends on the width of the stimulus θ_s. In Fig. 4 we plot time series for several values of θ_s, with $R_s\theta_s = r_s$ and $\vartheta = 0^\circ$. We see that with increasing θ_s the initial sharp negative ERP peak decreases in amplitude, but the existence of the peaks is robust. The decreasing amplitude is accounted for by the normalization of the stimulus in Eq. (52), which scales as θ_s^{-2}. A secondary effect is that the main peaks are slightly delayed as θ_s increases.

C. Dependence on ϑ

In Fig. 5 we explore the effect of ϑ (location on the sphere relative to the stimulus center) on the ERP time series for fixed $\theta_s = 3^\circ$. We observe that with increasing ϑ the negative ERP amplitude at $t \approx 85$ ms decreases. At $\vartheta = 0^\circ$ the time of the peak is 0.12 s with a $-50\,\mu$V ERP amplitude; the amplitude decreases monotonically to $-8.9\,\mu$V at $\vartheta = 180^\circ$, where the peak is delayed to 0.17 s. These trends are explained in terms of outward propagation of the ERP from $\vartheta = 0$, during which spreading and damping reduce the amplitude. A linear fit to the peak time versus ϑ yields propagation velocities of 6 m s^{-1} for the first negative peak and 10 m s^{-1} for the second, which are realistic phase velocities (which vary with frequency in general) for waves in the 10 Hz range implied by the temporal spacing of the peaks [77], and are comparable with the axonal velocity $\gamma_e r_e = 10$ m s^{-1} implied by Table I.

D. Modal dynamics in ERPs

In this section we explore the effects of eigenmode structure on the ERP time series. This is motivated by our recent work [78], which showed that some correlations which is low and runs from the crown of the head toward the ears

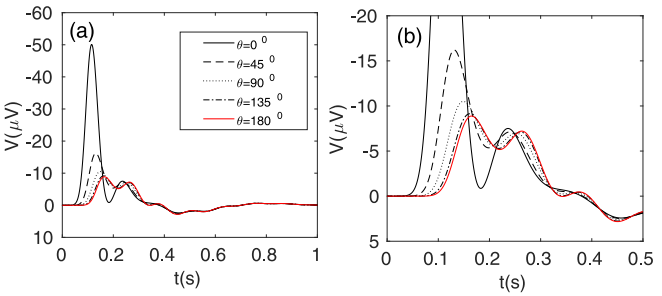

FIG. 5. ERP vs. ϑ, as indicated in the legend, for the parameters in Table I for spherical geometry with $\theta_s = 3^\circ$. (a) ERP time series. (b) Expanded view of (a) showing early times.

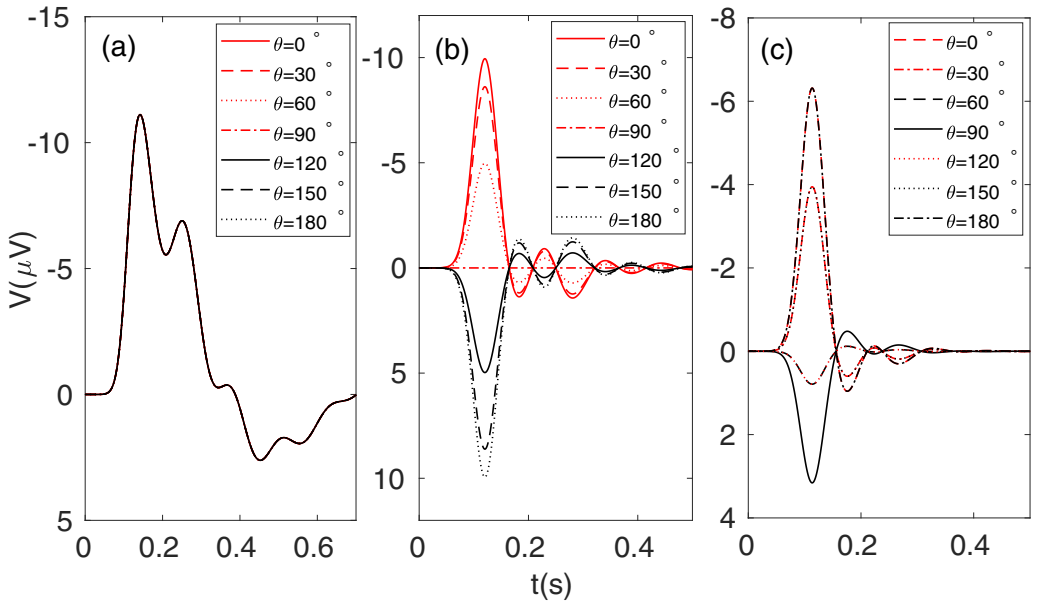

FIG. 6. Modal effects on theoretical ERP time series for the parameters in Table I from Eq. (67) for spherical geometry with $\theta_s = 3^\circ$. Time series are plotted for with different ϑ, as indicated in the legend. (a) $\ell = 0$, where all curves coincide because $Y_{00}(\vartheta, \varphi)$ is constant vs. ϑ and φ. (b) $\ell = 1$. (c) $\ell = 2$.

are dominated by very few modes. Prior work [49,72] also showed modal effects on white noise driven power spectra in planar and spherical geometries, especially near the alpha resonance and the low frequency resonance at $f = 0$, where they lead to large enhancements in responses, correlations, and coherence.

Figure 6(a) shows that the $\ell = 0$ contribution to the ERP is independent of ϑ, which is because $Y_{00}(\vartheta, \varphi)$ is constant. The peak occurs near the time of the total ERP at $\vartheta = 0$ in Fig. 5, but is only around a quarter as large. However, but that the largest positive amplitude near 0.5 s accounts for most of the total ERP amplitude at that time. At larger ϑ, Fig. 6(b) the $\ell = 0$ component is a larger fraction of the total ERP and can even exceed it in amplitude (which implies that the other components must partly cancel it). The $\ell = 1$ contribution to the ERP, showing that it exhibits more oscillations than $\ell = 0$, and its value is antisymmetric around $\vartheta = 90^\circ$, where it has a zero in accord with $Y_{10}^0 = (3/4\pi)^{1/2}\cos\vartheta$. This component has a slightly smaller peak amplitude than $\ell = 0$ and decays more rapidly in time. The corresponding results for $\ell = 2$ in Fig. 6(c) show a smaller amplitude at small ϑ than the previous cases, a more rapid fall-off with time, and an angular structure consistent with $Y_{20}^0 = (5/16\pi)^{1/2}(3\cos^2\vartheta - 1)$, has zeros at approximately 55° and 125°.

Overall, Fig. 6 shows the relative contributions of the first few eigenmodes to the ERP. These are explored in more detail in Fig. 7(a), which shows the individual contributions versus time at $\vartheta = 45^\circ$. We see that the modes add approximates in phase to produce the initial ERP peak, then progressively damp and dephase as time progresses; these effects give rise to the propagation of the total ERP across the sphere at its group velocity, as discussed in Sec. IV C. Figure 7(b) further illustrates this point by showing the cumulative totals up to a max $\ell = L_{\max}$ with $L_{\max} = 0, 1, 2, 5$. We see that retention of modes up to $L_{\max} \simeq 2$ is sufficient to represent the ERP on this case, although more modes would be required for very small θ_s at early times in order to accurately approximate the narrow initial ERP profile.

E. Parameter sensitivities

In this subsection we discuss sensitivities to the physiological parameters of the model, as shown in Fig. 8. Figure 8(a) shows the effect of the cortical damping rate γ_e. We see with increasing cortical damping γ_e, the amplitude is increased because increased γ_e restricts the response to a small area when r_e is held constant. Similar effects are seen in Fig. 8(b) for the decay rate α, with increasing α the initial peak increases in amplitude and becomes sharper because of reduced low-pass filtering in synapses and dendrites [36]. We see from Fig 8(c) that increasing the corticothalamic delay t_0 causes ERP features to be correspondingly delayed

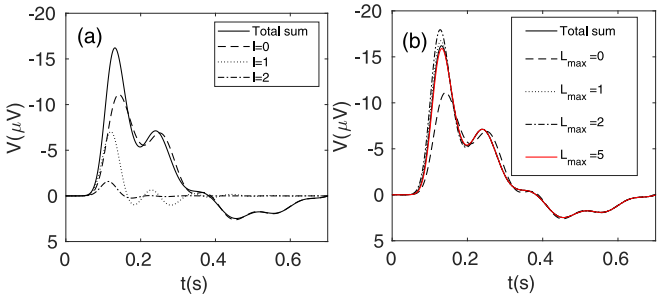

FIG. 7. Theoretical ERP time series for the parameters in Table I from Eq. (67) for spherical geometry with $\theta_s = 3^\circ$. (a) Time series are plotted for different ℓ contribution as indicated in the legend. (b) Time series are plotted for sums over ℓ up to various $L_{\max}$, as indicated in the legend.

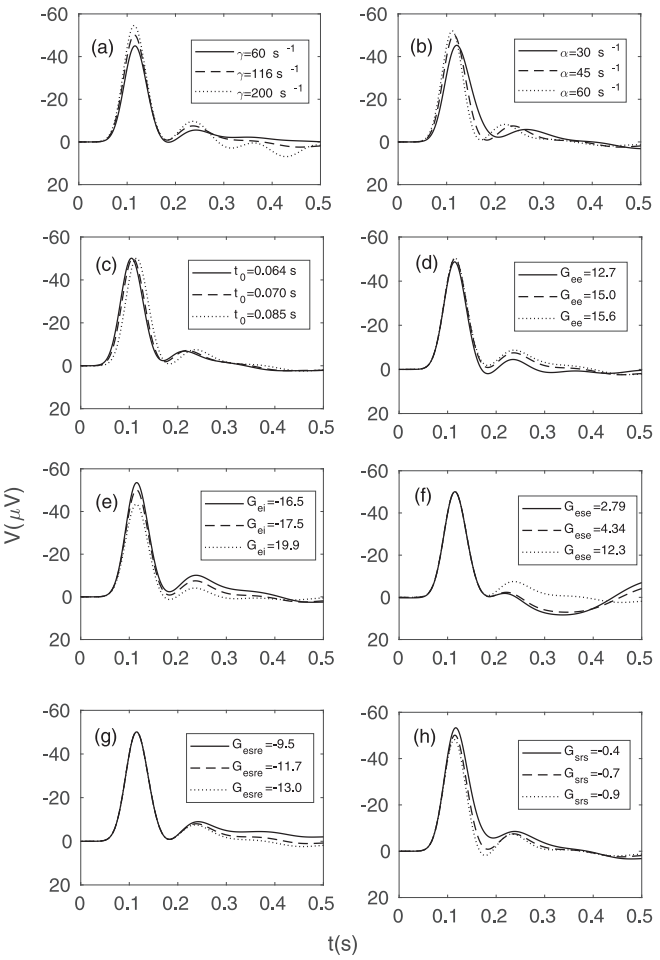

FIG. 8. Sensitivity of ERPs in spherical geometry to variation of model parameters, as labeled by the legend in the corner of the each frame. All cases here plotted for $\theta = 0^\circ$ and $\theta_s = 3^\circ$.

and to oscillate more slowly. Figures 8(d) and 8(e) show that the effects of the gains G_{ee} and G_{ei} are opposed, with increases in G_{ee} tending to increase the amplitude of the ERP, particularly at late times, where as increasing $|G_{ei}|$ tends to reduce amplitudes because G_{ei} is inhibitory; these results are in accord with previous work in the planar case [2]. Similarly, the corticothalamic loop gains G_{ese} and G_{esre} have opposite signs, so they also have opposing effects, as shown in Figs 8 (f) and (g), where the curves corresponding to increased G_{ese} are similar to the curves corresponding to decreased G_{erse}. Notably, the differences due to changing these gains are only seen after $t \approx 0.18$ s, when there has been sufficient time for signals to reach the cortex a second time after traversing the whole corticothalamic loop. The effect of changes of the inhibitory intrathalamic loop gain G_{srs} is seen from the time of the first ERP peak onward, where increasing $|G_{srs}|$ enhances intrathalamic oscillations [1,2,37]. Also increasing G_{srs} causes a deepened trough around $t \approx 0.19$ s [1].

V. SUMMARY AND DISCUSSION

We have used physiologically based neural field theory in infinite-planar and spherical cortical geometries to explore the effects of spherical topology and geometry on ERPs, modeled as responses to impulsive stimuli. In the spherical geometry, we explored ERPs using spherical-harmonic analysis [49,50,78]. The main results are:

(i) Neural field theory has been used to obtain a general transfer function for the corticothalamic system and we have calculated the ERP for infinite planar geometry and spherical geometry in Eqs. (45) and (67).

(ii) In the infinite planar case the target ERPs peak is sharp and negative, but in the spherical cases we get a stronger and sharper negative peaks due to the strong role of the uniform mode ($\ell = 0$) which contains a nonzero fraction of the total energy in the spatially finite case.

(iii) With increasing cortical radius R_s the spherical case approaches the infinite planar one, as expected on physical grounds.

(iv) Increasing the width of the stimulus θ_s decreases the ERP magnitude, mainly because the stimulus magnitude is reduced. There is also a slight delay in the timing of the ERP peaks.

(v) ERPs fall off with distance ϑ from the stimulus point due to damping and spreading. The velocity of the first peak is $\approx$6 m s^{-1} and the second peak is $\approx$10 m s^{-1}. Individual modal peaks are stationary and it is only when superposed that the resulting ERPs are seen to propagate at these group velocities.

(vi) Individual modal contributions to the total ERP fall off with ℓ, align in phase to produce the initial temporal peak, then dephase to produce the overall spatial propagation at the group velocity. Retention of modes with $L_{\max} \leqslant 2$ is sufficient to represent the ERP accurately, except at very small θ_s and t where the ERP is spatially narrow.

(vii) Sensitivities of the ERP to model parameters were explored and related to the physical effects they represent.

Overall, we find that discrete modal effects in spherical geometry are significant and are dominated by relatively few modes. Indeed only a handful of modes are needed to explain the main features of ERPs, in accord with recent numerical results that showed that just two modes could explain most features of experimentally evoked responses to random visual input stimuli [78]. By incorporating the correct cortical topology, the present analysis provides a bridge to the closely related modes on the fully convoluted cortex [50,61], and thus will also facilitate more realistic modeling and analysis of experimental brain signals in the future.

ACKNOWLEDGMENTS

This work was supported by a University of Sydney International Scholarship (USydIS), by the Australian Research Council Center of Excellence for Integrative Brain Function (ARC Grant No. CE140100007), and by the Australian Research Council Laureate Fellowship Grant No. FL140100025.

[1] C. J. Rennie, P. A. Robinson, and J. J. Wright, Biol. Cybern. **86**, 457 (2001).

[2] C. C. Kerr, C. J. Rennie, and P. A. Robinson, Biol. Cybern. **98**, 171 (2008).

[3] R. Näätänen and T. Picton, Psychophysiol. **24**, 375 (1987).
[4] T. W. Picton, S. Bentin, P. Berg, E. Donchin, S. A. Hillyard, R. Johnson, G. A. Miller, W. Ritter, D. S. Ruchkin, M. D. Rugg, M. and J. Taylor, Psychophysiol. **37**, 127 (2000).
[5] B. Kotchoubey, Prog. Brain Res. **150**, 427 (2005).
[6] S. Coombes, Biol. Cybern. **93**, 91 (2005).
[7] G. Deco, V. K. Jirsa, P. A. Robinson, M. Breakspear, and K. Friston, PLoS Comput. Biol. **4**, e1000092 (2008).
[8] B. Ermentrout, Rep. Prog. Phys. **61**, 353 (1998).
[9] W. J. Freeman, *Mass Action in the Nervous System* (Academic Press, New York, 1975).
[10] P. A. Robinson, C. J. Rennie, and D. L. Rowe, Phys. Rev. E **65**, 041924 (2002).
[11] P. A. Robinson, C. J. Rennie, and J. J. Wright, Phys. Rev. E **56**, 826 (1997).
[12] C. J. Rennie, P. A. Robinson, and J. J. Wright, Phys. Rev. E **59**, 3320 (1999).
[13] J. J. Wright and D. T. L. Liley, Behav. Brain Sci. **19**, 285 (1997).
[14] M. A. Buice and J. D. Cowan, Phys. Rev. E **75**, 051919 (2007).
[15] P. C. Bressloff and J. D. Cowan, Phys. D **173**, 226 (2002).
[16] S. I. Amari, Biol. Cybern **27**, 77 (1977).
[17] D. L. Rowe, P. A. Robinson, A. W. Harris, K. L. Felmingham, I. L. Lazzaro, and E. Gordon, J. Integr. Neurosci. **3**, 453 (2004).
[18] P. A. Robinson, R. W. Whitehouse, and C. J. Rennie, Phys. Rev. E **68**, 21922 (2003).
[19] J. A. Roberts and P. A. Robinson, Phys. Rev. E **85**, 011910 (2012).
[20] P. A. Robinson, Phys. Rev. E **72**, 011904 (2005).
[21] R. Srinivasan, S. Thorps, and P. L. Nunez, Front. Comput. Neurosci. **7**, 29 (2013).
[22] P. L. Nunez and R. Srinivasan, Brain Res. **1542**, 138 (2014).
[23] P. L. Nunez, R. Srinivasan, and R. D. Fields, Clin. Neurophysiol. **126**, 110 (2015).
[24] S. J. Van Albada, R. T. Gray, P. M. Drysdale, and P. A. Robinson, J. Theor. Biol. **257**, 664 (2009).
[25] M. Ferdousi, T. Janvier, and P. A. Robinson, J. Theor. Biol. **460**, 184 (2018).
[26] S. Assadzadeh and P. A. Robinson, R. Soc. Open Sci. **5**, 171952 (2018).
[27] C. C. Kerr, S. J. Van Albada, S. A. Neymotin, G. L. Chadderdon, P. A. Robinson, and W. W. Lytton, Front. Comput. Neurosci. **7**, 1 (2013).
[28] P. A. Robinson, C. J. Rennie, D. L. Rowe, S. C. O'Connor, and E. Gordon, Phil. Trans. R. Soc. B. **360**, 1043 (2005).
[29] P. A. Robinson, Phys. Rev. E **90**, 042712 (2014).
[30] P. A. Robinson, S. Postnova, R. G. Abeysuriya, J. W. Kim, J. A. Roberts, L. McKenzie-Sell, A. Karanjai, C. C. Kerr, F. Fung, R. Anderson, M. J. Breakspear, P. M. Drysdale, B. D. Fulcher, A. J. K. Phillips, C. J. Rennie, and G. Yin, A multiscale working brain model, in *Validating Computational Models in Neurological and Psychiatric Disorders*, edited by B. Bhattacharya and F. Chowdhury (Springer, New York, 2015).
[31] L. Ciganek, Clin. Neurophysiol. **13**, 165 (1961).
[32] S. F. Lopes, Electroencephalogr. Clin. Neurophysiol. **79**, 81 (1991).
[33] D. Mantini, M. G. Perrucci, G. C. Del, G. L. Romani, and M. Corbetta, Proc. Natl. Acad. Sci. USA **104**, 13170 (2007).
[34] H. Nordby, K. Hugdahl, R. Stickgold, K. Bronnick, and J. Hobson, NeuroReport **7**, 1082 (1996).
[35] P. A. Robinson, C. J. Rennie, D. L. Rowe, and S. C. O'Connor, Hum. Brain Mapp. **23**, 53 (2004).
[36] D. L. Rowe, P. A. Robinson, and C. J. Rennie, J. Theor. Biol. **231**, 413 (2004).
[37] M. Steriade, D. A. McCormick, and T. J. Sejnowski, Science **262**, 679 (1993).
[38] O. D. Creutzfeldt, S. Watanabe, and H. D. Lux, Electroencephalogr. Clin. Neurophysiol. **20**, 1 (1966).
[39] H. Davis, P. A. Davis, A. L. Loomis, E. N. Harvery, and G. Hovert, J. Neurophysiol. **2**, 500 (1939).
[40] C. C. Kerr, C. J. Rennie, and P. A. Robinson, J. Neurosci. Meth. **179**, 101 (2009).
[41] W. D. Penny, S. J. Kiebel, J. M. Kilner, and M. D. Rugg, Trends Neurosci. **25**, 387 (2002).
[42] D. M. Regan, Electroencephalogr. Clin. Neurophysiol. **20**, 238 (1989).
[43] G. Pfurtscheller and F. Lopes da Silva, Clin. Neurophysiol. **110**, 1842 (1999).
[44] J. Harsh, U. Voss, J. Hull, S. Schrepfer, and P. Badia, Psychophysiol. **31**, 244 (1994).
[45] M. S. Zobaer, R. M. Anderson, C. C. Kerr, P. A. Robinson, K. K. H. Wong, and A. L. D'Rozario, Biol. Cybern. **111**, 149 (2017).
[46] P. L. Nunez, *Neocortical Dynamics and Human EEG Rhythms* (Oxford University Press, New York, 1995).
[47] D. Bouattoura, P. Gaillard, P. Villon, and F. Langevin, Med. Biol. Eng. Comput. **36**, 415 (1998).
[48] P. Valdès, J. Bosch, R. Grave, J. Hernandez, J. Riera, R. Pascual, and R. Biscay, Brain Topogr. **4**, 309 (1992).
[49] K. N. Mukta, J. N. MacLaurin, and P. A. Robinson, Phy. Rev. E **96**, 052410 (2017).
[50] P. A. Robinson, X. Zhao, K. M. Aquino, J. D. Griffiths, S. Sarkar, and G. Mehta-Pandejee, NeuroImage **142**, 79 (2016).
[51] R. A. Yotter, R. Dahnke, P. M. Thompson, and C. Gaser, Hum. Brain Mapp. **32**, 1109 (2011).
[52] R. Srinivasan, P. L. Nunez, and R. B. Silberstein, IEEE Trans. Biomed. Eng. **45**, 814 (1998).
[53] L. Shen and M. K. Chung, in *Proceedings of the 3rd International Symposium on 3D Data Processing, Visualization and Transmission, IEEE Comp. Soc., Chapel Hill, NC* (Wiley, New York, 2006), p. 294.
[54] C. Brechbühler, G. Geirg, and O. Kübler, Comp. Vis. Image Understand. **61**, 154 (1995).
[55] G. Gerig, M. Styner, D. Jones, D. Weinberger, and J. Lieberman, in *Proceedings of the IEEE Workshop on Mathematical Methods in Biomedical Image Analysis, Hawaii* (Wiley, New York, 2001), p. 171.
[56] B. Gutman, Y. Wang, L. M. Lui, T. F. Chan, and P. M. Thompson, in *Proceedings of the 18th International Conference on Pattern Recognition, Hong Kong* (Wiley, New York, 2006), p. 964.
[57] A. Kelemen, G. Szekely, and G. Gerig, IEEE Trans. Med. Imag. **18**, 828 (1999).
[58] M. E. Shenton, G. Gerig, R. W. McCarley, G. Székely, and R. Kikinis, Psych. Res. **115**, 15 (2002).
[59] P. M. Thompson and A. W. Toga, Trans. Med. Imag. **15**, 402 (1996).
[60] R. G. Abeysuriya, C. J. Rennie, P. A. Robinson, and J. W. Kim, Clin. Neurophysiol. **125**, 2016 (2014).

[61] N. C. Gabay and P. A. Robinson, Phy. Rev. E **96**, 032413 (2017).
[62] C. C. Kerr, C. J. Rennie, and P. A. Robinson, Clin. Neurophysiol. **122**, 134 (2011).
[63] H. R. Wilson and J. D. Cowan, Kybernetik **13**, 55 (1973).
[64] X. Zhao, J. W. Kim, and P. A. Robinson, J. Theor. Biol. **370**, 93 (2015).
[65] D.-P. Yang and P. A. Robinson, Phy. Rev. E **95**, 042410 (2017).
[66] T. B. Janvier and P. A. Robinson, Front. Hum. Neurosci. **12**, 334 (2018).
[67] M. L. Steyn-Ross, D. A. Steyn-Ross, and J. W. Sleigh, Cong. Neurod. **6**, 215 (2012).
[68] P. Sanz-Leon, P. A. Robinson, S. A. Knock, P. M. Drysdale, R. G. Abeysuriya, F. K. Fung, C. J. Rennie, and X. Zhao, PLoS Comp. Biol. **14**, e1006387 (2018).
[69] F. H. Lopes da Silva, A. Hoeks, H. Smits, and L. H. Zetterberg, Kybernetik **15**, 27 (1974).
[70] R. G. Abeysuriya and P. A. Robinson, J. Neurosci. Meth. **258**, 28 (2016).
[71] R. G. Abeysuriya, C. J. Rennie, and P. A. Robinson, J. Neurosci. Meth. **253**, 55 (2015).
[72] P. A. Robinson, P. N. Loxley, S. C. O'Connor, and C. J. Rennie, Phys. Rev. E **63**, 041909 (2001).
[73] R. G. Abeysuriya, C. J. Rennie, and P. A. Robinson, J. Theor. Biol. **344**, 70 (2014).
[74] P. L. Nunez and R. Srinivasan, Clin. Neurophysiol. **117**, 2424 (2006).
[75] F. W. J. Olver, D. W. Lozier, R. F. Boisvert, and C. W. Clark, *NIST Handbook of Mathematical Functions* (Cambridge University Press, Cambridge, 2010), p. 428, Sec. 2.17.5, Eq. (2).
[76] A. P. Prudnikov, Yu. A. Brychkov, and O. I. Marrichev, *Integrals and Series* (Gordon and Breach, New York, 1986), Vol. 2.
[77] P. A. Robinson, P. C. Chen, and L. Yang, Biol. Cybern. **98**, 1 (2008).
[78] P. A. Robinson, J. C. Pagès, N. C. Gabay, T. Babaie, and K. N. Mukta, Phys. Rev. E **97**, 042418 (2018).